Periodic Migration in a Physical Model of Cells on Micropatterns

Brian A. Camley,[1,2] Yanxiang Zhao,[2,3] Bo Li,[2,3] Herbert Levine,[4] and Wouter-Jan Rappel[1,2]

[1]*Department of Physics, University of California, San Diego, La Jolla, California 92093, USA*
[2]*Center for Theoretical Biological Physics, University of California, San Diego, La Jolla, California 92093, USA*
[3]*Department of Mathematics, University of California, San Diego, La Jolla, California 92093, USA*
[4]*Department of Bioengineering, Center for Theoretical Biological Physics, Rice University, Houston, Texas 77005, USA*

(Received 6 June 2013; published 10 October 2013)

We extend a model for the morphology and dynamics of a crawling eukaryotic cell to describe cells on micropatterned substrates. This model couples cell morphology, adhesion, and cytoskeletal flow in response to active stresses induced by actin and myosin. We propose that protrusive stresses are only generated where the cell adheres, leading to the cell's effective confinement to the pattern. Consistent with experimental results, simulated cells exhibit a broad range of behaviors, including steady motion, turning, bipedal motion, and periodic migration, in which the cell crawls persistently in one direction before reversing periodically. We show that periodic motion emerges naturally from the coupling of cell polarization to cell shape by reducing the model to a simplified one-dimensional form that can be understood analytically.

DOI: 10.1103/PhysRevLett.111.158102 PACS numbers: 87.17.Jj, 02.70.−c, 87.17.Aa

Cultured cells on two-dimensional substrates are often used as a convenient proxy for more biologically relevant situations, such as cells within a three-dimensional extracellular matrix (ECM). However, cells in the ECM often exhibit qualitatively different modes of migration than those on substrates [1–4]. A remarkable example of this is the discovery of periodic migration in zyxin-depleted cells in a collagen matrix [5]. Understanding cell motility in the ECM may be profoundly important for the study of cancer invasion [6]. Interestingly, features of cell morphology and dynamics in a matrix are recapitulated in cells on micropatterned adhesive substrates, including cell speed, shape, dependence on myosin [1], and periodic migration [5]. Other micropatterns induce cell polarization and directed cell motion [7–9] and sorting of cells from one- to two-dimensional regions of micropatterns [10]. In this Letter, we study the influence of micropatterns on cell motility using an extension of a computational model of eukaryotic cell crawling [11,12] and observe a wide range of dynamic behaviors including periodic migration. To our knowledge, ours is the first cell crawling simulation to display periodic migration.

It would be natural to expect that periodic migration [5] requires underlying oscillatory protein dynamics, as in Min oscillations in *E. coli* [13]. Surprisingly, this is not the case; periodic migration and other complex behaviors appear with only minimal alteration to the model for freely crawling cells. We study periodic migration in detail, and show that it is a consequence of feedback between the cell's shape and its biochemical polarization, i.e., how proteins are segregated to one side of the cell. We use sharp interface theory to reduce our model to a simplified 1D model that is analytically tractable. Periodic migration exemplifies how coupling between cell shape and chemical polarity can lead to unexpected cell behavior.

Model summary.—We describe the cell's cytoskeleton as a viscous, compressible fluid driven by active stresses from actin polymerization and myosin contraction. This is appropriate for the long time scales of keratocyte and fibroblast migration on which the cytoskeleton can rearrange; see, e.g., Ref. [14]. Our model is one of a broad spectrum of active matter [15,16] models of motility in which active stresses drive deformation [14,17–26]. Details of the model are available in Ref. [12]; we review it briefly to highlight changes made to study cells on micropatterns. It has four modules: (1) cell shape, tracked by a phase field $\phi(\mathbf{r}, t)$, (2) the cytoskeleton as an active viscous compressible fluid [14,27], (3) actin promoter (e.g., Rac or Cdc42) and myosin concentrations obeying reaction-diffusion-advection equations, and (4) adhesions between cell and substrate, tracked individually.

Cell shape is tracked by a "phase field" $\phi(\mathbf{r}, t)$ that is zero outside and unity inside the cell [11,28–33]. ϕ varies smoothly across the cell boundary, which is implicitly set by $\phi = 1/2$. $\phi(\mathbf{r}, t)$ obeys

$$\partial_t \phi + \mathbf{u} \cdot \nabla \phi = \Gamma(\epsilon \nabla^2 \phi - G'(\phi)/\epsilon + c\epsilon|\nabla \phi|) \quad (1)$$

where $\mathbf{u}$ is the cytoskeletal velocity, Γ a relaxation coefficient, $c = \nabla \cdot (\nabla \phi/|\nabla \phi|)$ is the local interface curvature, ϵ the interface width, and $G(\phi) = 18\phi^2(1-\phi)^2$.

We describe cytoskeletal flow with a Stokes equation including active forces from actin and myosin and forces induced by membrane curvature and cell-substrate adhesion:

$$\nabla \cdot [\nu(\nabla \mathbf{u} + \nabla \mathbf{u}^T)] + \nabla \cdot (\sigma_{\text{poly}} + \sigma_{\text{myo}}) + \mathbf{F}_{\text{mem}} + \mathbf{F}_{\text{adh}} - \xi \mathbf{u} = 0, \quad (2)$$

where $\nu(\phi) = \nu_0\phi$ is the viscosity. ξ does not vary over the substrate; i.e., $\xi\mathbf{u}$ is a hydrodynamic drag [34], not friction from adhesive binding [35]. Individual adhesions lead to $\mathbf{F}_{\rm adh}$; $\mathbf{F}_{\rm mem}$ comes from membrane deformations (see Supplemental Material [36]). We neglect the pressure term arising from coupling between cytoskeletal mesh and cytoplasm [14]. Equation (2) is solved numerically with a semi-implicit finite difference spectral method; other equations are stepped explicitly (see Supplemental Material [36]).

Our central hypothesis for the effect of the adhesive micropattern is that protrusive stress from actin polymerization $\sigma_{\rm poly}$ is only generated where the cell contacts the micropattern,

$$\sigma_{\rm poly} = -\eta_a^0\chi(\mathbf{r})\phi\rho_a\delta_\epsilon\hat{\mathbf{n}}\,\hat{\mathbf{n}}, \quad (3)$$

where $\chi(\mathbf{r})$ is one inside the pattern and zero outside, $\delta_\epsilon(\phi) = \epsilon|\nabla\phi|^2$, $\hat{\mathbf{n}}$ is the normal to the cell surface, ρ_a the actin promoter density on the membrane, and η_a^0 a protrusion coefficient. Our assumption is supported by experimental work showing that fibroblasts preferentially protrude processes from points near newly formed adhesions, which only form on the pattern [37]. Others have proposed active stresses proportional to cell-substrate adhesion [38]. Our pattern is a stripe, $\chi(\mathbf{r}) = (1/2)\times[1 + \tanh(3\{(w/2) - |x|\}/\epsilon)]$, with w the stripe width. The contractile stress is $\sigma_{\rm myo} = \eta_m^0\phi\rho_m\mathbf{I}$, with ρ_m the myosin density, η_m^0 the myosin contractility coefficient, and $\mathbf{I}$ the identity tensor.

Cell polarization arises from ρ_a, which follows a wave-pinning model [39]. The actin promoter exchanges between active membrane-bound (ρ_a) and inactive cytosolic ($\rho_a^{\rm cyt}$) states; the membrane-bound promoter catalyzes binding to the membrane. Fronts between high ρ_a and low ρ_a can stall ("pin"), leading to a steady polarization [39].

Actin promoter and myosin processes only occur inside the cell; the phase field method is ideally suited to handle reaction-diffusion-advection equations within moving cells [11,19,31–33]. The reaction-diffusion-advection equations for the actin promoter and myosin are

$$\partial_t(\phi\rho_a) + \nabla\cdot(\phi\rho_a\mathbf{u}) = \nabla\cdot[\phi D_a\nabla\rho_a] + \phi f, \quad (4)$$

$$\partial_t(\phi\rho_m) + \nabla\cdot(\phi\rho_m\mathbf{u}) = \nabla\cdot[\phi D_m(\rho_a)\nabla\rho_m]. \quad (5)$$

The actin promoter diffuses with coefficient D_a on the membrane; at this level of modeling, we do not distinguish between membrane and cytoskeleton velocity, and so ρ_a is advected with the cytoskeletal velocity $\mathbf{u}$. Myosin binds and unbinds from the cytoskeleton, which we model as a ρ_a-dependent diffusion coefficient $D_m(\rho_a) = D_m^0/(1 + \rho_a/K_D)$ [12]. The nonlinear reaction term $f(\rho_a, \rho_a^{\rm cyt})$ for promoter membrane-cytosol exchange is in the Supplemental Material [36]. $\rho_a^{\rm cyt}$ is well mixed (constant) and set by the conservation of ρ_a; i.e., $\int d^2r\phi(\mathbf{r})[\rho_a(\mathbf{r}) + \rho_a^{\rm cyt}] = N_a^{\rm tot}$ is constant.

Adhesions between cell and substrate are formed, age, and transition between modes as in [12]. However, adhesions may only form on the micropattern [37]; adhesions that leave the micropattern are destroyed (see Supplemental Material [36]). The number of adhesions is fixed. We do not enforce symmetry, unlike Ref. [12].

Simulation of periodic migration.—Numerical evaluation of Eqs. (1)–(5) shows spontaneous emergence of periodic motion. An initially circular cell contracts to the stripe, polarizes, migrates one way, then reverses and migrates in the other direction. We present one reversal in Fig. 1. When the cell is polarized (ρ_a is segregated on one side), the cell contracts while crawling in the direction of its polarization [point (a) in Fig. 1]. As the cell contracts, it depolarizes [1(b)]. The unpolarized cell expands quickly, but does not crawl significantly. As the cell grows, it suddenly repolarizes [1(c)] and begins to travel in the direction opposite to its initial direction. As the cell moves, myosin localizes to the cell rear [40], and the cell begins to contract again [1(d)]. Each reversal corresponds to one peak in the cell area.

Several questions arise. (1) How does cell polarization control the cell's growth and contraction? (2) Why does the cell depolarize at small areas and repolarize at large ones? (3) Why does the cell repolarize in a direction *opposite* to its original motion? We address these questions by reducing our model to a significantly simpler 1D one.

Reduction to 1D model.—We neglect adhesions and advection of ρ_a. The latter is not strictly justified, as the Peclet number $\mathrm{Pe} = V_{\rm cell}L_{\rm cell}/D_a$ is of order unity ($L_{\rm cell}$ is

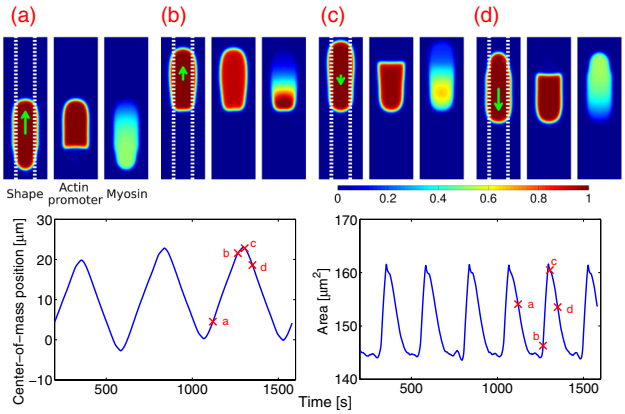

FIG. 1 (color online). Top: Cell shape (ϕ), actin promoter ($\rho_a\phi$), and myosin ($\rho_m\phi$) distribution at four time points (a)-(d) during a reversal event in periodic migration. Color plots are rescaled by unity, 1.4 μm^{-2} and 0.55 μm^{-2}, respectively. Cell velocity is indicated by an arrow. Total width of stripe is $w = 6$ μm (dashed lines). Bottom: Center-of-mass position [$\bar{y} = (1/A)\int d^2ry\phi(x, y)$] and area ($A = \int d^2r\phi$) of cell as a function of time. Full parameters for all simulations are listed in the Supplemental Material [36].

the cell length and $V_{\rm cell}$ its velocity), but we reproduce the essential aspects of the two-dimensional simulation without fluid flow. In migrating cells, myosin accumulates at the back while actin is enriched at the front [40]. We model these myosin dynamics phenomenologically by letting myosin go to the cell rear (where ρ_a is low) with time lag τ. The simplified model for ρ_a and ρ_m is

$$\partial_t(\phi\rho_a) = \partial_y[\phi D_a \partial_y \rho_a] + \phi f(\rho_a, \rho_a^{\rm cyt}), \tag{6}$$

$$\partial_t \rho_m^{f,b} = -\tau^{-1}[\rho_m^{f,b} - (m_0 - \rho_a^{f,b})], \tag{7}$$

where $\rho_{a,m}^{f,b} = \rho_{a,m}(y_{f,b})$ and m_0 is the equilibrium myosin when ρ_a is zero. The cell "front" is defined by $y_f > y_b$. The cell shape is $\phi(y,t) = (1/2)[\tanh(3(y-y_b)/\epsilon) - \tanh(3(y-y_f)/\epsilon)]$. Actin polymerization causes local protrusion; myosin contraction causes local contraction. The simplest form for the normal velocity of the edge is thus $\mathbf{v}_{\rm edge}\cdot\hat{\mathbf{n}} = \alpha\rho_a - \beta\rho_m$; i.e.,

$$\partial_t y_{f,b} = \pm(\alpha\rho_a^{f,b} - \beta\rho_m^{f,b}). \tag{8}$$

This result can be rigorously justified in some limits by solving the Stokes equation [Eq. (2)] in the presence of a planar front. If $\epsilon/\ell_h \ll 1$ (sharp interface limit) and $L_{\rm cell} \gg \ell_h$, where $\ell_h = \sqrt{2\nu_0/\xi}$, we find $\alpha = \eta_a^0/4\nu_0$ and $\beta = \eta_m^0\ell_h/2\nu_0$ (see Supplemental Material [36]).

This limit is not necessarily applicable, as we have $\ell_h \approx 63\ \mu{\rm m} > L_{\rm cell}$. Nevertheless, Eqs. (6)–(8) capture the essential features of periodic migration in Fig. 1. We simulate them (Fig. 2) and compare the 1D simulation to the center line of Fig. 1.

Our 1D model shows how the cell's shape changes and polarization are coupled. The cell shrinks if $\partial_t L_{\rm cell} = \partial_t(y_f - y_b) = \alpha(\rho_a^f + \rho_a^b) - \beta(\rho_m^f + \rho_m^b)$ is negative. To find when this is true, we need $\rho_a^{f,b}$. We use the analysis of Mori *et al.* [39,41], who proposed the wave-pinning reaction-diffusion model we apply in Eq. (6). Their solutions would be exact if $\epsilon \to 0$ (sharp interface limit) and the cell were slow moving, Pe $\ll 1$. Pe is not small, but these solutions provide a valuable qualitative guide to the cell's polarization as a function of its size. We use the simplified reaction kinetics $\tilde{f}(\rho_a, \rho_a^{\rm cyt}) \equiv -k\rho_a(\rho_a - h)(\rho_a - m\rho_a^{\rm cyt})$, which reproduce the phenomenology of the full kinetics and permit analytical solutions. h and m are parameters related to the steady states of ρ_a [39]. Mori *et al.* find two homogeneous and linearly stable steady states, $\rho_a(y) = 0$ and $\rho_a(y) = mN_a^{\rm tot}/L_{\rm cell}(1+m)$, where $N_a^{\rm tot} = \int_0^L dy(\rho_a + \rho_a^{\rm cyt})$ is the conserved total number of actin promoter molecules in either the membrane-bound or cytosolic form [$N_a^{\rm tot} = \int d^d r(\rho_a + \rho_a^{\rm cyt})\phi$ in the phase field model]. Reference [39] also finds a polarized state with a stationary front connecting a region with $\rho_a = 2h$ to $\rho_a = 0$; the length of the region with large ρ_a is $y_p = (N_a^{\rm tot}/2h) - (L_{\rm cell}/m)$. The cell can only polarize if $y_p < L_{\rm cell}$, i.e., $L_{\rm cell} > L_{\rm depol} \equiv mN_a^{\rm tot}/2h(m+1)$. This causes the cell to depolarize at small lengths, partially answering question (2) above.

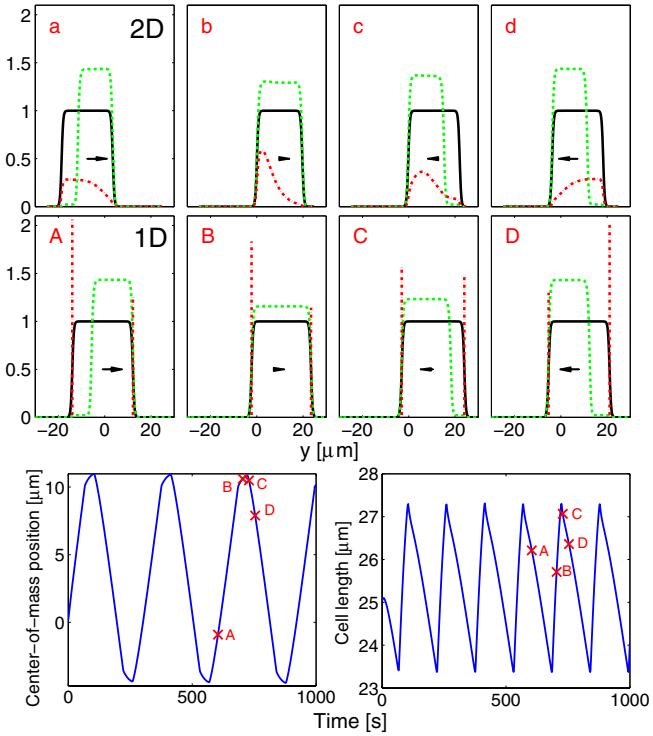

FIG. 2 (color online). Two- and one-dimensional models show highly similar behavior. Top: Center line of Fig. 1 a–d with ϕ (black solid line), $\phi\rho_a$ (green dashed line), and $\phi\rho_m$ (red dash-dotted line); axis is shifted for comparison to middle plot, Middle: 1D model at comparable points in the periodic cycle (A)–(D). Bottom: Plot of position and size of periodically migrating 1D cell.

Why does the cell not immediately repolarize when $L_{\rm cell} > L_{\rm depol}$? The homogeneous state $\rho_a(y) = mN_a^{\rm tot}/L_{\rm cell}(1+m)$ is linearly stable; even though the cell can support a polarized state if $L_{\rm cell} > L_{\rm depol}$, it will not reach that state without a perturbation beyond a certain threshold. Numerically evaluating Eq. (6) in a cell of fixed size, we find that this threshold decreases with increasing cell size; larger cells are easier to polarize. [For the full kinetics $f(\rho_a, \rho_a^{\rm cyt})$, this threshold can decrease to zero [41].] Others [42–44] have also suggested that cell shape influences signaling, polarization, and response to stimuli.

What perturbation causes the cell's repolarization? Within the 1D model the only possibility is the moving edge. If a cell edge expands faster than ρ_a can be transported by diffusion or converted from cytosolic form, ρ_a will be depleted near the expanding edge. Explicitly, if we numerically solve Eq. (6) for an initially homogeneous cell with one edge expanding, the cell always polarizes to a state with low ρ_a near the expanding edge. Depletion sets the direction in which the repolarization occurs. As the cell expands, both edges have high ρ_a, but one has lower ρ_m (Figs. 1 and 2). The edge normal velocity is set by Eq. (8):

actin polymerization causes expansion, but local contraction from myosin decreases the edge's velocity. Therefore, the edge with low ρ_m expands faster, leading to more depletion of ρ_a near that edge. When this depletion crosses the threshold of patterning, a polarized state forms with low ρ_a near the quickly moving edge, and high ρ_a near the slowly moving edge: the cell polarizes in the direction of higher myosin. Myosin keeps the memory of the cell's direction: if it becomes uniform before the cell repolarizes, this information is lost.

We have now answered our questions from above. (1) Cell shape is set by ρ_a and ρ_m via Eq. (8), and this is controlled by the cell polarization. (2) At small cell sizes, Eq. (6) does not support a polarized state, but as the cell expands, the polarized state and homogeneous state are both stable. Polarization requires a perturbation to ρ_a larger than a threshold, which decreases as the cell grows. (3) Repolarization is initiated by depletion of ρ_a near an expanding cell boundary; myosin makes the previous "back" of the cell expand more slowly, ensuring the cell polarizes in a direction opposite to its previous movement.

We calculate the amplitude of periodic migration analytically by using the results of [39] and making some additional assumptions. We assume the cell depolarizes at length L_{depol} as above and repolarizes in the direction of high myosin at a critical length L^*. The value of L^* would depend on the details of the cell's motion, the diffusion coefficient D_a, and the threshold for perturbations. We expect that the dominant contribution to the cell's displacement over time will be the distance that it crawls while polarized; when the cell is polarized, it contracts. We can then approximate the amplitude of periodic migration as $A = v_{\mathrm{c.m.}} t_{\mathrm{contract}}$, where $v_{\mathrm{c.m.}}$ is the cell center of mass velocity in the contraction phase, and t_{contract} the time required to contract from L^* to L_{depol}. Using Eq. (8) and the results of [39], we find that in the polarized state, $\partial_t L_{\mathrm{cell}} \approx 2h\alpha - \beta(2m_0 - 2h)$ (assuming the myosin is at its equilibrium value $\rho_m = m_0 - \rho_a$). Similarly, $v_{\mathrm{c.m.}} \approx h(\alpha + \beta)$. We find

$$A = \left(\frac{L^* - L_{\mathrm{depol}}}{2}\right)\frac{\gamma + 1}{\gamma_c - \gamma}, \tag{9}$$

where $\gamma = \alpha/\beta$ and $\gamma_c = (m_0 - h)/h$. For the cell to contract while polarized, $\gamma < \gamma_c$. The cell must also grow while unpolarized for periodic migration to occur; this condition depends on N_a^{tot}.

For the amplitude of periodic migration to become large, protrusion and retraction must be balanced so that $\gamma - \gamma_c$ is small. However, this requirement can be weakened by the cell's internal dynamics, which we have mostly neglected in deriving Eq. (9). If we assume a large viscous resistance to changes in size, we suppress the rate of contraction and expansion by a factor λ, where $\lambda \ll 1$. If the cell's contraction is slowed, but crawling is not, the amplitude of periodic migration increases significantly, as $t_{\mathrm{contract}} \sim 1/\lambda$, and $A \approx t_{\mathrm{contract}} v_{\mathrm{c.m.}}$, so $A \sim 1/\lambda$ becomes large.

Additional emergent behaviors.—Depending on initial conditions and micropattern width, other behaviors are observed. These include steady crawling, turning, and bipedal motion (see Supplemental Material [36]). The bipedal motion resembles that seen theoretically and experimentally by Barnhart *et al.* [45]. Turning has been studied by Rubinstein and co-workers [46,47]; see also Ref. [19]. We plan to address the origin of these effects within our model in future work.

If periodic migration in [5] arose through precisely the mechanism we have described, the cell area would oscillate with a period half that of the cell's migration and myosin reorientation would lag the reversal of cell direction (Figs. 1 and 2). It would be interesting to experimentally quantify total surface area and myosin localization of periodically migrating cells. We present this study primarily as an example of complex behaviors that develop when cell polarization is coupled to cell shape. However, our mechanism of periodic migration may be more general if cell polarization is coupled to other mechanical properties. Cell-surface adhesion is a natural choice, as periodic motion arises in [5] when the adhesion protein zyxin is depleted. If cells only polarize when sufficiently adherent to the surface, and this adhesion changes with cell motion, our periodic migration scheme may be recapitulated with adhesion in place of cell area.

Periodic migration as observed in our simulations is a new, interesting, and tractable example of the complex dynamics resulting from coupling cell shape and polarity. Periodic migration requires a balance between contraction and protrusion [Eq. (9)], but its existence is robust to many model details. Within our larger model, individual adhesions can be neglected, as can the ρ_a dependence of D_m. In the 1D model, we have ignored hydrodynamics entirely. Removing features or varying parameters (see Supplemental Material [36]) changes migration amplitude, but if the fundamental aspects illustrated by the 1D model are present, periodic migration exists. Therefore, we believe periodic migration could be observed in other models of eukaryotic cell motility that couple polarity and cell shape [11,26,32,44,48], especially those using the wave-pinning polarity mechanism [39]. Randomly occurring reversals without periodicity have been observed by Ziebert and Aronson [49]; their model may only lack a memory. Our one-dimensional model suggests the essential elements required for periodic migration, and emphasizes the role of myosin in preserving the memory of the cell's initial direction. Our model for cells on adhesive micropatterns and the analytical tools we developed to study periodic migration may be useful in understanding more complex behavior on micropatterns, including "dimension sensing" [10], response of fibroblasts to cross-hatched patterns [1], and polarization in response to

asymmetric micropatterns [7–9]. In all of these cases, cell polarity is coupled to the underlying micropattern. The coupling of micropattern shape, cell shape, and cell polarization studied here will be essential to a deeper understanding of these problems.

This work was supported by NIH Grants No. P01 GM078586 and No. R01 GM096188, NSF Grant No. DMS 1309542, and by the Center for Theoretical Biological Physics.

[1] A. Doyle, F. Wang, K. Matsumoto, and K. Yamada, J. Cell Biol. **184**, 481 (2009).
[2] R. Poincloux, O. Collin, F. Lizárraga, M. Romao, M. Debray, M. Piel, and P. Chavrier, Proc. Natl. Acad. Sci. U.S.A. **108**, 1943 (2011).
[3] M. H. Zaman, L. M. Trapani, A. L. Sieminski, D. MacKellar, H. Gong, R. D. Kamm, A. Wells, D. A. Lauffenburger, and P. Matsudaira, Proc. Natl. Acad. Sci. U.S.A. **103**, 10 889 (2006).
[4] D. Yamazaki, S. Kurisu, and T. Takenawa, Oncogene **28**, 1570 (2009).
[5] S. I. Fraley, Y. Feng, A. Giri, G. D. Longmore, and D. Wirtz, Nat. Commun. **3**, 719 (2012).
[6] D. Wirtz, K. Konstantopoulos, and P. C. Searson, Nat. Rev. Cancer **11**, 512 (2011).
[7] T. Vignaud, L. Blanchoin, and M. Théry, Trends Cell Biol. **22**, 671 (2012).
[8] M. Théry, V. Racine, M. Piel, A. Pépin, A. Dimitrov, Y. Chen, J.-B. Sibarita, and M. Bornens, Proc. Natl. Acad. Sci. U.S.A. **103**, 19 771 (2006).
[9] G. Mahmud, C. J. Campbell, K. J. Bishop, Y. A. Komarova, O. Chaga, S. Soh, S. Huda, K. Kandere-Grzybowska, and B. A. Grzybowski, Nat. Phys. **5**, 606 (2009).
[10] S. S. Chang, W.-h. Guo, Y. Kim, and Y.-l. Wang, Biophys. J. **104**, 313 (2013).
[11] D. Shao, W.-J. Rappel, and H. Levine, Phys. Rev. Lett. **105**, 108104 (2010).
[12] D. Shao, H. Levine, and W.-J. Rappel, Proc. Natl. Acad. Sci. U.S.A. **109**, 6851 (2012).
[13] J. Lutkenhaus, Annu. Rev. Biochem. **76**, 539 (2007).
[14] B. Rubinstein, M. Fournier, K. Jacobson, A. Verkhovsky, and A. Mogilner, Biophys. J. **97**, 1853 (2009).
[15] F. Juelicher, K. Kruse, J. Prost, and J.-F. Joanny, Phys. Rep. **449**, 3 (2007).
[16] M. Marchetti, J.-F. Joanny, S. Ramaswamy, T. Liverpool, J. Prost, M. Rao, and R. A. Simha, Rev. Mod. Phys. **85**, 1143 (2013).
[17] P. Recho, T. Putelat, and L. Truskinovsky, Phys. Rev. Lett. **111**, 108102 (2013).
[18] R. J. Hawkins, M. Piel, G. Faure-Andre, A. M. Lennon-Dumenil, J.-F. Joanny, J. Prost, and R. Voituriez, Phys. Rev. Lett. **102**, 058103 (2009).
[19] E. Tjhung, D. Marenduzzo, and M. E. Cates, Proc. Natl. Acad. Sci. U.S.A. **109**, 12 381 (2012).
[20] C. A. Whitfield, D. Marenduzzo, R. Voituriez, and R. J. Hawkins, arXiv:1307.3426.
[21] A. Callan-Jones and R. Voituriez, New J. Phys. **15**, 025022 (2013).
[22] M. Herant and M. Dembo, Biophys. J. **98**, 1408 (2010).
[23] J.-F. Joanny and S. Ramaswamy, J. Fluid Mech. **705**, 46 (2012).
[24] K. Kruse, J.-F. Joanny, F. Jülicher, and J. Prost, Phys. Biol. **3**, 130 (2006).
[25] R. Voituriez, J.-F. Joanny, and J. Prost, Phys. Rev. Lett. **96**, 028102 (2006).
[26] C. W. Wolgemuth, J. Stajic, and A. Mogilner, Biophys. J. **101**, 545 (2011).
[27] J. S. Bois, F. Jülicher, and S. W. Grill, Phys. Rev. Lett. **106**, 028103 (2011).
[28] J. Kockelkoren, H. Levine, and W.-J. Rappel, Phys. Rev. E **68**, 037702 (2003).
[29] W. Boettinger, J. Warren, C. Beckermann, and A. Karma, Annu. Rev. Mater. Res. **32**, 163 (2002).
[30] J. B. Collins and H. Levine, Phys. Rev. B **31**, 6119 (1985).
[31] T. Biben, K. Kassner, and C. Misbah, Phys. Rev. E **72**, 041921 (2005).
[32] F. Ziebert, S. Swaminathan, and I. S. Aranson, J. R. Soc. Interface **9**, 1084 (2012).
[33] X. Li, J. Lowengrub, A. Rätz, and A. Voigt, Commun. Math. Sci. **7**, 81 (2009).
[34] E. Evans and E. Sackmann, J. Fluid Mech. **194**, 553 (1988).
[35] S. Walcott and S. X. Sun, Proc. Natl. Acad. Sci. U.S.A. **107**, 7757 (2010).
[36] See Supplemental Material at http://link.aps.org/supplemental/10.1103/PhysRevLett.111.158102 for additional simulations, tables of parameters, extended derivations, and details of numerical methods.
[37] N. Xia, C. K. Thodeti, T. P. Hunt, Q. Xu, M. Ho, G. M. Whitesides, R. Westervelt, and D. E. Ingber, FASEB J. **22**, 1649 (2008).
[38] A. Carlsson, New J. Phys. **13**, 073009 (2011).
[39] Y. Mori, A. Jilkine, and L. Edelstein-Keshet, Biophys. J. **94**, 3684 (2008).
[40] Myosin is swept to the cell rear by the retrograde cytoskeletal flow, as **u** is less than the cell velocity through most of the cell; see Ref. [12].
[41] Y. Mori, A. Jilkine, and L. Edelstein-Keshet, SIAM J. Appl. Math. **71**, 1401 (2011).
[42] J. Meyers, J. Craig, and D. J. Odde, Curr. Biol. **16**, 1685 (2006).
[43] W. R. Holmes, B. Lin, A. Levchenko, and L. Edelstein-Keshet, PLoS Comput. Biol. **8**, e1002366 (2012).
[44] A. F. Marée, V. A. Grieneisen, and L. Edelstein-Keshet, PLoS Comput. Biol. **8**, e1002402 (2012).
[45] E. L. Barnhart, G. M. Allen, F. Jülicher, and J. A. Theriot, Biophys. J. **98**, 933 (2010).
[46] A. Mogilner and B. Rubinstein, J. Phys. Condens. Matter **22**, 194118 (2010).
[47] B. Rubinstein, K. Jacobson, and A. Mogilner, Multiscale Model. Simul. **3**, 413 (2005).
[48] W. R. Holmes and L. Edelstein-Keshet, PLoS Comput. Biol. **8**, e1002793 (2012).
[49] F. Ziebert and I. S. Aronson, PLoS One **8**, e64511 (2013).